Molecular Biology of the Cell
Vol. 12, 4013–4029, December 2001

Actin Filaments and Myosin I Alpha Cooperate with Microtubules for the Movement of Lysosomes[V]

Marie-Neige Cordonnier,* Daniel Dauzonne,† Daniel Louvard,* Evelyne Coudrier*‡

Centre National de la Recherche Scientifique,* Morphogenèse et Signalisation Cellulaires, Unité Mixte de Recherche 144, Institut Curie; †Unité Mixte de Recherche 176, Institut Curie, 75248 Paris Cedex 05, France

Submitted July 27, 2001; Revised July 27, 2001; Accepted September 6, 2001
Monitoring Editor: J. Richard McIntosh

An earlier report suggested that actin and myosin I alpha (MMIα), a myosin associated with endosomes and lysosomes, were involved in the delivery of internalized molecules to lysosomes. To determine whether actin and MMIα were involved in the movement of lysosomes, we analyzed by time-lapse video microscopy the dynamic of lysosomes in living mouse hepatoma cells (BWTG3 cells), producing green fluorescent protein actin or a nonfunctional domain of MMIα. In GFP-actin cells, lysosomes displayed a combination of rapid long-range directional movements dependent on microtubules, short random movements, and pauses, sometimes on actin filaments. We showed that the inhibition of the dynamics of actin filaments by cytochalasin D increased pauses of lysosomes on actin structures, while depolymerization of actin filaments using latrunculin A increased the mobility of lysosomes but impaired the directionality of their long-range movements. The production of a nonfunctional domain of MMIα impaired the intracellular distribution of lysosomes and the directionality of their long-range movements. Altogether, our observations indicate for the first time that both actin filaments and MMIα contribute to the movement of lysosomes in cooperation with microtubules and their associated molecular motors.

INTRODUCTION

Lysosomes are acidic organelles delimited by a single membrane and contain a characteristic set of hydrolases. Their size is comprised between 0.3 and 0.5 μm with an electron dense core. They are the final site of accumulation of internalized molecules, and they play an important role in the degradation of intracellular molecules. Recent electron microscopic morphological analyses and in vitro cell free assays showing heterotypic fusion between late endosomes and lysosomes suggest that late endosomes may fuse with lysosomes in the perinuclear region (Stoorvogel *et al.*, 1991; Futter *et al.*, 1996; Mullock *et al.*, 1998; Bucci *et al.*, 2000; Luzio *et al.*, 2000). In addition to their function of intracellular digestion, experimental evidence in hematopoietic cells and several other cell types indicates that lysosomes are involved in secretion and are thus able to fuse with the plasma membrane (Andrews, 2000). The fact that lysosomes might fuse in the perinuclear region with late endosomes, and at the cell periphery with the plasma membrane, suggests that they are highly dynamic and able to move from the perinuclear region to the cell periphery and vice versa.

It is well accepted that microtubules and associated molecular motors are responsible for intracellular movements of organelles and vesicles. Matteoni and Kreis (1987) were the first to observe that lysosomes move on microtubules. The movement of lysosomes has been shown to require cytoplasmic dynein and kinesin (Hollenbeck and Swanson, 1990; Aniento *et al.*, 1993; Bananis *et al.*, 2000). More recently, actin filaments have also been implicated in the maintenance of the steady state distribution of endosomes and lysosomes, as well as in membrane trafficking between these two organelles (Van Deurs *et al.*, 1995; Durrbach *et al.*, 1996a; Liu *et al.*, 1997; Barois *et al.*, 1998). The molecular mechanism underlying the requirement of actin in endocytosis might be based upon the ability of endosomes and lysosomes to nucleate actin assembly and rocket at the tip of dynamic actin comet tails (Merrifield *et al.*, 1999; Taunton *et al.*, 2000). In addition to actin, molecular motors associated with actin, such as myosins, might be involved in this molecular mechanism, as we proposed in an earlier review (Coudrier *et al.*, 1992). In fact, class I myosins have been implicated in different aspects of the endocytic pathway in a variety of organisms. The yeast class I myosins, and homologues of these myosins in amoebae and *Aspergilus nidulans,* have been

‡ Corresponding author. E-mail address: coudrier@curie.fr.
[V] Online version of this article contains video material for Figures 2, 5, 7, and 9. Online version is available at www.molbiolcell.org.

proposed to act at the first stage of endocytosis during vesicle formation by reorganizing the cortical actin network (Novak *et al.*, 1995; Ostap and Pollard, 1996; Jung *et al.*, 1996; Geli and Riezman, 1996; Yamashita and May, 1998). Moreover, it has recently been shown that the yeast class I myosins can participate in actin assembly (Evangelista *et al.*, 2000; Geli *et al.*, 2000; Lee *et al.*, 2000, Jung *et al.* 2001). Other members of class I myosins are involved in later steps of endocytosis: the deletion of myoB in *dictyostellium* induces defects in fluid phase endocytosis, oversecretion of lysosomal enzymes, and reduced membrane recycling, while a mammalian member of this family (myosin I alpha), associated with endosomes and lysosomes, regulates the delivery of internalized molecules to lysosomes (Temesvari *et al.*, 1996; Raposo *et al.*, 1999, Neuhaus and Soldati 2000). Altogether, these observations suggest that the recruitment of cytosolic actin on the membrane of lysosomes might contribute to push these organelles throughout the cytoplasm, and that members of class I myosins might participate in this recruitment. Alternatively, class I myosins might exert a force on actin filaments to move lysosomes, or to temporarily immobilize them on actin filaments and thereby control their movements.

To discriminate between these hypotheses, we analyzed by time-lapse video microscopy the movement of lysosomes in living mouse hepatoma cells (BWTG3 cells) producing green fluorescent protein tagged actin (GFP-actin) or a nonfunctional domain of myosin I alpha (MMIα). All together, our observations indicate for the first time that actin filaments cooperate with microtubules for the movement of lysosomes in hepatoma cells, and that a myosin from class I is implicated in this process.

MATERIALS AND METHODS

Antibodies

We used a mAb H68.4 directed against the cytoplasmic tail of the transferrin receptor, according to White *et al.* (1992), and polyclonal antibodies raised against the amino terminus of Myr 1, the mouse orthologue of MMIα, and referred to as Tü 29 (Ruppert *et al.*, 1993). The mAb directed against Lamp1 was obtained from PharMingen (Los Angeles, CA), and the mAb directed against GFP from Roche (Meylan, France).

Recombinant cDNA Constructions and Transfection

The recombinant plasmid encoding GFP-MMIαΔn295 was obtained by deleting the fragment *Bam*HI–*Bam*HI from the recombinant plasmid encoding GFP-Myr 1b, the mouse orthologue of MMIα, according to Raposo *et al.* (1999). The expression of the recombinant plasmid led to the addition of 12 amino acids (SGLRSRAQASNS) between the GFP protein and MMIα truncated protein (aa 296-1041). The recombinant plasmid encoding GFP β-actin was a generous gift from B. Imhof (Ballestrem *et al.*, 1998). Transfection with recombinant DNAs was performed with 10 μg of the appropriate DNA for five millions cells according to Raposo *et al.* (1999). After 24 h, cells were supplemented with 0.7 mg/ml Geneticin, (Life Technologies, Paisley, Scotland) and were permanently grown in this medium. Three stable cellular clones producing GFP-MMIαΔn295 were selected by immunofluorescence after cloning. More than 80% of the cells produce the recombinant protein in the clone that we are currently using. Cellular clones of mock cells were obtained by transfection of BWTG3 cells with the pEGFP vector without any insert and were selected similarly to GFP-MMIαΔn295 expressing cells. GFP-actin cells were kept as a pool of Geneticin resistant cells, to obtain different levels of expression of the protein in different cells of the same culture.

Cell Culture

The mouse hepatoma cell line BWTG3 (Szpirer and Szpirer, 1975) or cellular clones producing GFP-MMIαΔn295, GFP β-actin, or mock cells were grown at 37°C under 10% CO_2 in Coon's F-12 modified medium (Seromed, Berlin, Germany) supplemented with 10% FCS (Seromed). Penicillin (10 U/ml) and streptomycin (10 mg/ml; Seromed) were added to the medium in the case of wild-type cells, while cellular clones were grown in presence of Geneticin. Cellular clones producing GFP-MMIαΔn295, GFP β-actin, or mock cells were incubated overnight with 10 mM sodium butyrate before analysis

Immunofluorescence Microscopy

Cells were fixed with 3% paraformaldehyde and 0.025% glutaraldehyde, permeabilized with PBS containing 0.1% saponin, and analyzed by indirect immunofluorescence. Cells were first incubated 30 min with primary antibodies, followed by 30 min with Alexa 488 conjugated secondary antibodies (Molecular Probes, Eugene, OR). Cells were viewed with a confocal laser-scanning microscope (Leica, Heidelberg, Germany).

Membrane Fractionation and Immunoblotting

Cells were grown for 5 d in 175-cm^2 flasks, collected by scraping, and resuspended in 1 ml homogenization buffer containing 10 mM triethanolamine, pH 7.4, 0.25 M sucrose, 1 mM EDTA, and a protease inhibitor cocktail from Sigma (St. Louis, MO). They were then homogenized by passing them twice through a 22G 1′1/4 gauge needle. Unbroken cells and nuclei were removed from the cell homogenate by centrifugation at 1000 × *g* for 10 min, and the crude membrane fraction contained in the postnuclear supernatant (PNS) was loaded in 25% Percoll, on a 1 M sucrose cushion according to the method of Green *et al.* (1987). After centrifugation for 20 min at 22,500 × *g*, collected fractions were assayed for β-hexosaminidase and alkaline phosphodiesterase activities before being combined in three pools as described in Raposo *et al.* (1999).

Proteins from the different fractions were separated by SDS-PAGE and were transferred onto nitrocellulose membranes in the presence of 20 mM Tris, 150 mM glycine, and 0.0375% SDS. Antibody detection was performed using the chemiluminescence blotting substrate from Boehringer Mannheim (Mannheim, Germany).

Chemical Synthesis of Pepstatin A-BODIPY-TR-cadaverine Hydrochloride (BODIPY-TR Pepstatin A)

N-hydroxysuccinimide (2.32 mg, 0.0201 mmol) and 1,3-dicyclohexylcarbodiimide (3.78 mg, 0.0183 mmol) were successively added to a stirred solution of pepstatin A (Sigma, 12.55 mg, 0.0183 mmol) in anhydrous DMF (3 ml). The mixture was stirred overnight under Argon at room temperature, until the complete disappearance of the starting pepstatin A, as judged by TLC (using a mixture of dichloromethane/methanol 8:2 as eluent and by examining the plates with a phosphomolybdic acid spray). Commercial 5-[((4-(4,4-difluoro-5-(2-thienyl)-4-bora-3a,4a-diaza-s-indacene-3-yl)phenoxy)acetyl)amino]pentylamine hydrochloride (BODIPY-TR-cadaverine hydrochloride, 10 mg, 0.0183 mmol), purchased from Molecular Probes was then added in one portion. An excess of triethylamine (40 μl), dried by distillation over calcium hydride before use, was next introduced into the reaction medium *via* a syringe to liberate the free amine. The mixture was further stirred at room temperature under Argon for 16 additional hours. Removal of the volatile compounds under reduced pressure followed by flash-chromatography (employing a mixture dichloromethane/methanol 8:2 as eluent) provided, after evaporation of the solvents, 19.78 mg (92%) of the satisfac-

torily pure wanted fluorescent probe as a deep blue powder. MS-FAB : *m/z* 1199 $(M + Na)^+$.

Internalization of BODIPY-TR Pepstatin A and Drug Treatments

GFP-actin and GFP-MMIαΔn295 producing cells were grown for 1 or 2 d respectively on 25 mm diameter coverslips before incubation with 1 μM BODIPY-TR pepstatin A for 90 min at 37°C in culture medium. The coverslips were then washed three times in culture medium and were mounted in a small open chamber (BELLCO Glass.) with 1.5-ml culture medium. The small open chamber was introduced into a 37°C, 5% CO_2 regulated chamber on microscope stage and was covered with a removable membrane, selectively permeable for gas. A 20-min chase with culture medium was then performed under the microscope before starting acquisition.

In the case of the drug treatments, 1 ml culture medium was added to the mounted cells, and one control series of sequential images was acquired. Then 500 μl culture medium containing nocodazole, cytochalasin D, or latrunculin A, was immediately added to the sample under the microscope for a final drug concentration of 1 μM, 1 μM, and 0.5 μM, respectively. A series of sequential images of the same cell and other cells were taken after 10 min (nocodazole, cytochalasin D) or 5 min (latrunculin A) of incubation. Nocodazole incubation time was determined to permit perturbation of microtubules without perturbing actin filaments, as judged by immunofluorescence using anti-tubulin antibody and phalloidin (our unpublished results). Similarly, actin drugs incubation times were chosen to permit perturbation of the actin cytoskeleton without perturbing microtubules. The number of images per series was set at 31 in order to be able to make two series of images of the same cell, for example before and after drug treatment, without perturbing the cell with too strong illumination.

Time-lapse Video Microscopy

The movement of pepstatin A filled compartments in BWTG3 cells was monitored using a Leica inverted microscope (Leica) equipped with a Plan Apochromat 100 × 1.4 NA oil immersion lens. A motorized fluorescence filter wheel was used to observe Texas Red (N21 excitation BP 515–560, dichroïque 565, emission LP 590) and GFP (L5 excitation BP480/40, dichroïque 505, emission BP 527/30) sequentially. Illumination was provided by a halogen lamp through a green filter for phase contrast observations, or by a 50W HBO mercury burner for fluorescence. All the images were captured using a Princeton cooled CCD camera (Micromax, Princeton Instrument, Trenton, NJ), controlled by Metamorph software (Universal Imaging, Media, PA), at a rate of one couple of GFP/Texas Red frames (200 ms and 100 ms exposures ,respectively) every 6 s. The switch between GFP and Texas Red fluorescence and an external shutter limiting light exposition of the sample were also controlled by Metamorph software.

Image Analysis

The position of 60–150 fluorescent particles was hand determined in successive frames, using Metamorph software even for small tubules as their size did not exceed a few pixels. The corresponding coordinates of fluorescent particles at a given time were stored and allowed to calculate distance d(i) and speed [d(i)/Δt] between consecutive particle positions, where Δt is the time-lapse between frames (Δt = 6s). Maximum displacement dmax as the largest distance that the particle could cover from its initial point and maximum speed vmax as the highest speed between consecutive particle positions were also calculated using Sigma Plot software (SPSS, Chicago, IL). To graph the histograms showing the distribution of dmax and vmax, the values of dmax and vmax were rounded to the closest entire or tenth value respectively. We defined the persistence (p) of a moving particle as the ratio between the distance covered by the particle and the distance between its initial and final points:

$$p = \Sigma[d(\mathrm{i})]/d(AB) \quad (1)$$

where A and B are the initial and final points of the particle trajectory, and d(AB) the distance between A and B.

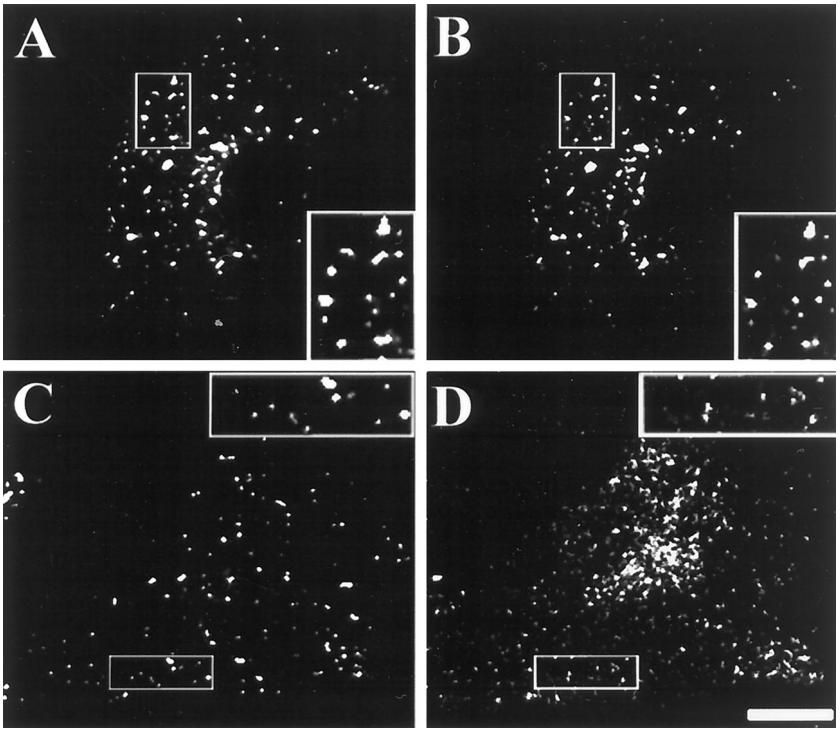

Figure 1. Subcellular distribution of BODIPY-TR pepstatin A in BWTG3 cells. After internalization for 90 min of BODIPY-TR pepstatin A and a 20-min chase at 37°C, fixed and permeabilized cells were labeled with anti-Lamp1 (B), or anti-transferrin receptor (D) antibodies. (A, B) Distribution of BODIPY-TR pepstatin A and Lamp1 respectively on a confocal section near the cell base. (C, D) Distribution of BODIPY-TR pepstatin A and transferrin receptor respectively on a confocal section near the cell base. Bar = 10 μm. Inserts show higher magnification

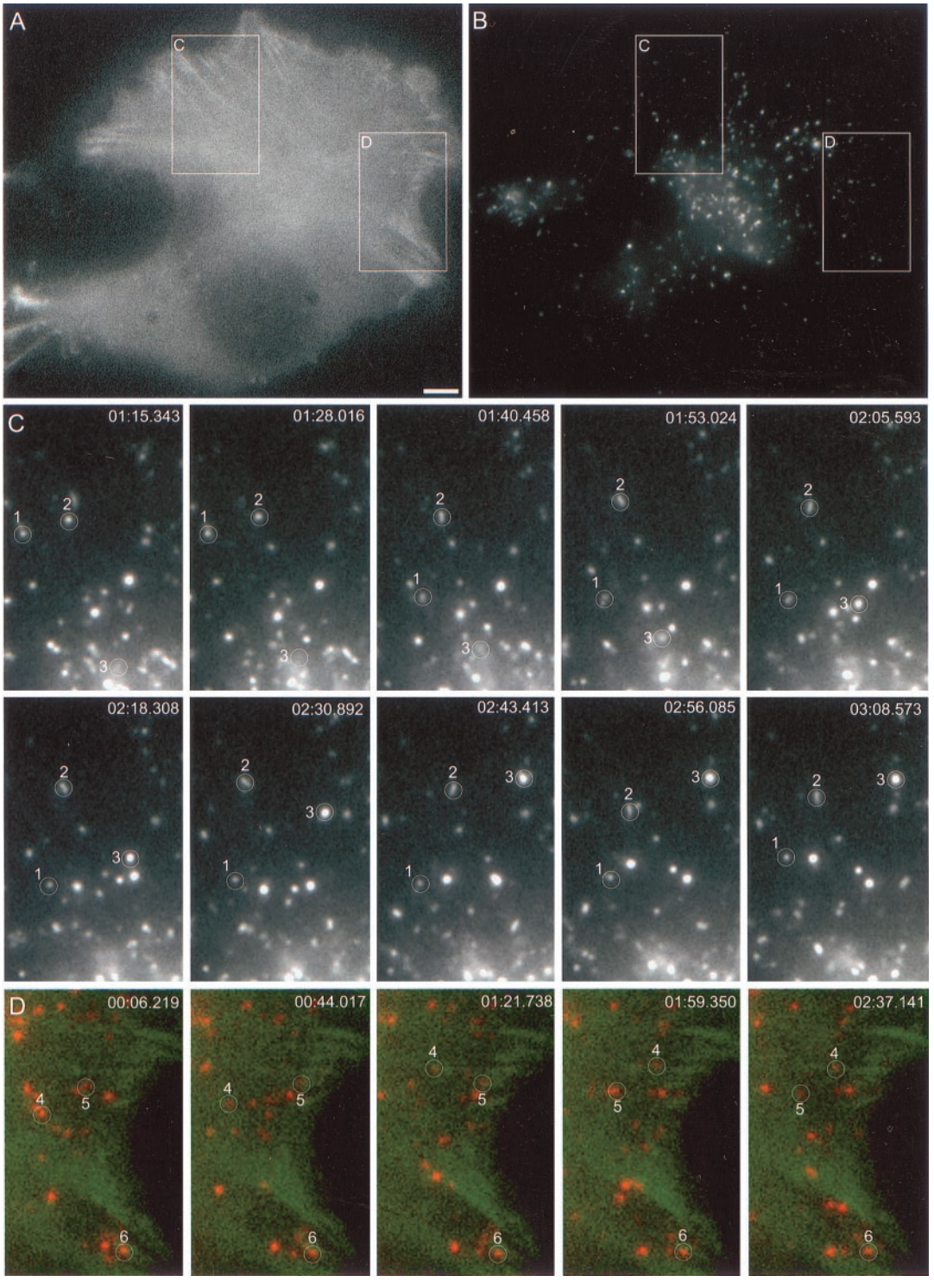

Figure 2. Analysis of BODIPY-TR pepstatin A-filled compartment movements in a cell producing GFP-actin by time-lapse video microscopy. Thirty-one couples of GFP/Texas Red images were captured at a rate of one couple every 6 s, for a cell producing GFP-actin after BODIPY-TR pepstatin A internalization. (A) First GFP-actin frame of the time-lapse sequence. (B) First BODIPY-TR pepstatin A frame of the time-lapse sequence. (C) BODIPY-TR pepstatin A time-lapse sequence in a part of the cell shown in panels A and B at a rate of one image every 12 s (the exact time is given on the pictures), showing different types of movements. Particle number 1 exhibits a combination of short random and rapid directional movements, particle number 2 transiently elongates and performs short random movements, and particle number 3 undergoes a rapid long-range directional movement. (D) BODIPY-TR pepstatin A (red) and GFP-actin (green) time-lapse sequence

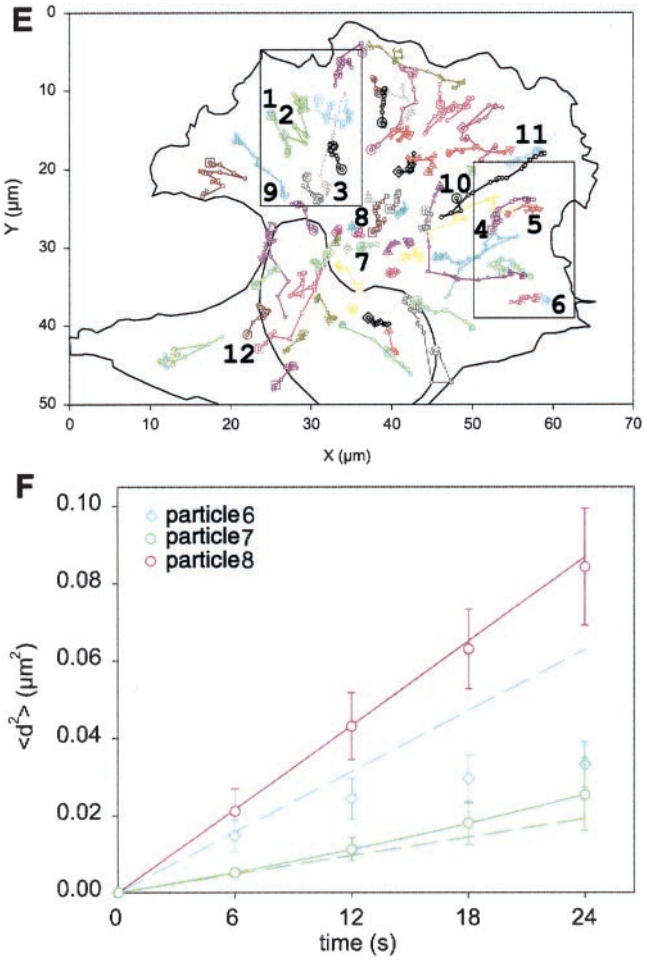

Figure 2 (cont.) in a part of the cell shown in panels A and B, at a rate of 1 image every 12 s, showing one BODIPY-TR pepstatin A-filled compartment going toward an actin cable and stopping there (particle number 4), another one stopping on an actin cable and escaping (particle number 5), and a region rich in F-actin containing several immobile BODIPY-TR pepstatin A- filled compartments, including particle number 6. (E) Examples of trajectories of BODIPY-TR pepstatin A-filled compartments in the cell shown in A and B (colored lines and dots). For clarity, a set of colors and dot shapes was assigned to each particle; a bigger dot shows the beginning of each track. The outlines of the cell and its nucleus were represented (continuous lines) from a phase contrast image taken at the beginning of the time-lapse sequence. Numbers in the black rectangles point out the corresponding particles followed in (C) and (D). Numbers 7 and 8 show examples of trajectories of oscillating lysosomes, numbers 9, 10, 11, and 12 show examples of centripetal and centrifugal trajectories respectively. (F) Examples of mean square displacements (dots with error bars) and corresponding fits (continuous lines) with Equation (2) for a lysosome undergoing diffusive motion (number 8), and a lysosome undergoing diffusive and directed motion (number 7). The mean square displacement of a confined lysosome is also shown (number 6). It cannot be fitted with equation (2). Dashed lines are straight lines to emphasize the curvature of the mean square displacement of particles 6 (blue) and 7 (green). For clarity, mean square displacement of particles 7 and 8 were divided by 10 before plotting. Bar = 5 μm.

Random motions of particles were characterized by their mean square displacement as a function of time, $<d^2(t)>$. According to Abney *et al.* (1999), $<d^2(t)>$ was calculated and fitted using Sigma Plot software to a model equation displaying two terms, the first one describing diffusive motions, and the second one describing a directed motion:

$$\langle d^2(t)\rangle = 4Dt + v^2t^2 \quad (2)$$

where, d is the displacement, t the time, D the diffusion coefficient, and v the speed of the particle in the model. Brackets $< >$ denote averaging, performed as described by Abney *et al.* (1999). Error bars were calculated as SEs of the averaging.

RESULTS

The Majority of Pepstatin A Filled Compartments Codistributes with Lysosomes in BWTG3 Cells

Pepstatin A inhibits and binds specifically cathepsin D a major lysosomal aspartic endopeptidase and can be used as a tracer of lysosomes (Chen *et al.*, 2000). To follow the movement of lysosomes in living cells producing GFP-tagged proteins, we synthesized Pepstatin A conjugated covalently to BODIPY-TR cadaverine hydrochloride (BODIPY-TR pepstatin A). After internalization of the fluorescent peptide and chase, BWTG3 cells displayed a punctate staining throughout the cytoplasm. These vesicle-like structures strictly colocalized with Lamp 1, which we have previously shown to label lysosomes of this hepatoma cell line at the electron microscopic level (Raposo *et al.* 1999)(Figure 1A and B). Their intracellular distribution is strikingly different from the distribution of transferrin receptor, a marker for early endosomes and recycling compartments (Figure 1C and D). These observations indicate that the majority of the pepstatin A-loaded compartments correspond to lysosomes. Therefore, we used BODIPY-TR pepstatin A in these conditions to monitor the movement of lysosomes in living cells.

Lysosomes Undergo a Combination of Rapid Directional Movements on Microtubules and Short Random Movements and Pauses, Sometimes on Actin Filaments

To follow lysosomes and actin at the same time, we analyzed by time-lapse video microscopy the dynamic of internalized BODIPY-TR pepstatin A in BWTG3 cells stably expressing GFP-actin. We observed a labeling typical of peripheral actin cables in the thinner regions of these cells (Figure 2A). These filamentous structures could also be labeled with rhodamine-phalloïdin after fixation and permeabilization of cells (our unpublished results). In addition, we observed a diffuse staining likely due to a loose dense network of microfilaments or to a pool of monomeric GFP-actin in the cytoplasm (Figure 2A). This diffuse GFP-actin pool was recruited to actin filamentous structures after jasplakinolide treatment, suggesting that the GFP-actin from this cytosolic pool was able to be incorporated into actin filaments, as previously observed by Ballestrem *et al.* (1998) (our unpublished results).

Pepstatin A-filled compartments were dispersed in the cytoplasm of live cells similarly to their distribution observed in fixed cells (Figure 2B vs. Figures 1A, 1C). The movements and the distribution of these compartments in

Table 1. Quantification of lysosomes movements in GFP-actin and GFP-MMIαΔn295 expressing cells

	Percent lysosomes with dmax <2.5 μm (total no. lysosomes)	Confined lysosomes (% of total)	Percent lysosomes with v > 0.3 μm/s
GFP-actin no. 1[a]	34 (91)	21	47
GFP-actin no. 2[b]	37 (95)	27	52
GFP-actin no. 3[c]	31 (104)	19	56
GFP-actin nocodazole[d]	93 (154)	80	0
GFP-actin cytochalasin D no. 1[e]	65 (96)	50	33
GFP-actin cytochalasin D no. 2	82 (80)	56	12
GFP-actin cytochalasin D no. 3	81 (67)	51	10
GFP-MMIαΔn295 no. 1[f]	41 (71)	28	44
GFP-MMIαΔn295 no. 2	37 (65)	32	51
GFP-MMIαΔn295 no. 3[c]	29 (89)	29	56
GFP-MMIαΔn295 nocodazole[d]	94 (86)	85	0

[a] Same cell as in Figure 2.

[b] Cell of Figure 5 before cytochalasin D treatment.

[c] Same cell as in Figure 11 before nocodazole treatment.

[d] Same cell as in Figure 11 after nocodazole treatment.

[e] Same cell as in Figure 5.

[f] Same cell as in Figure 9.

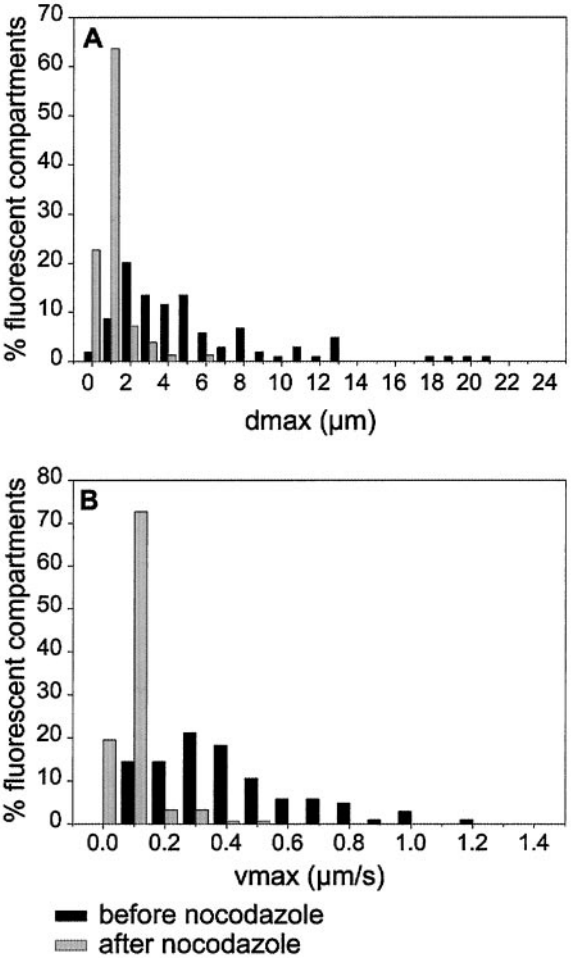

Figure 3. Analysis of the distribution of maximal displacements and maximum speeds recorded for BODIPY-TR pepstatin A-filled compartments of a cell producing GFP-actin, before and after addition of nocodazole. (A) and (B) show respectively the distribution of maximal displacements *dmax* for a period of time of 3 min and the distribution of maximum speeds *vmax*, before (black bars) and after (gray bars) nocodazole treatment. 104 and 154 fluorescent particles were tracked before and after drug treatment, respectively. The number of fluorescent particles with a given *dmax* or *vmax* is calculated as a percentage of the total number of fluorescent particles analyzed.

GFP-actin expressing cells were comparable to those observed in nontransfected cells or in cells producing GFP (our unpublished results). Mostly vesicular, pepstatin A-filled compartments transiently elongated in small tubules (Figure 2C, and video 2C particle no. 2). Trajectories analysis revealed that most of these compartments were undergoing a combination of rapid long directional movements, short random movements, and pauses (Figure 2C, and video 2C particles nos. 1 and 3, see also the corresponding trajectories on Figure 2E).

The rapid long directional movements were observed in both centrifugal and centripetal directions between the cell center and the periphery (Figure 2E particles 9 and 10 for centripetal movements, and particles 11 and 12 for centrifugal movements). The addition of nocodazole, a drug that depolymerizes microtubules, completely eliminated these directed motions, whereas short random movements were still observed in these conditions (Figure 11B vs. Figure 11A). Therefore, we assume that the rapid bidirectional movements observed here are microtubule-dependent, as previously described by several other groups (Matteoni and Kreis, 1987; Prekeris *et al.*, 1999). After nocodazole treatment, all the lysosomes had speeds inferior to 0.3 μm/s. In addition, only 7% of them could go further than 2.5 μm from their initial tracking point after 3 min., vs. 63–69% in nontreated cells (Table 1, Figure 3, A and B). We chose $v = 0.3$ μm/s and $dmax = 2.5$ μm for 3 min as arbitrary limits to separate microtubule-dependent speeds from others and from nocodazole sensitive trajectories, respectively. Approximately 50% of the lysosomes were moving at least once with a speed higher than 0.3 μm/s in nontreated cells (Table 1 and Figure 3B). The average of microtubule-dependent speeds, calculated as the mean of the speeds superior to 0.3 μm/s, and the maximum speed of long-range directional lysosomes (lysosomes going further than 6.5 μm from their initial tracking point) were 0.46 ± 0.02 μm/s and 0.66 ± 0.06 μm/s, respectively, for the cell shown in Figure 2 and similar for other cells analyzed under the same conditions (the mean of the speeds superior to 0.3 μm/s for 150 lysosomes taken from 3 different cells was 0.45 ± 0.01 μm/s).

In each GFP actin expressing cells analyzed, ~34% of lysosomes didn't move further than 2.5 μm from their initial tracking point (Table 1, Figure 3A). ~95% of these lysosomes had speeds inferior to 0.3 μm/s, and none of them exhibited long-range directional movements. The average and maximum speed of these lysosomes with random motion were 0.026 ± 0.002 μm/s and 0.12 ± 0.01 μm/s, respectively, for

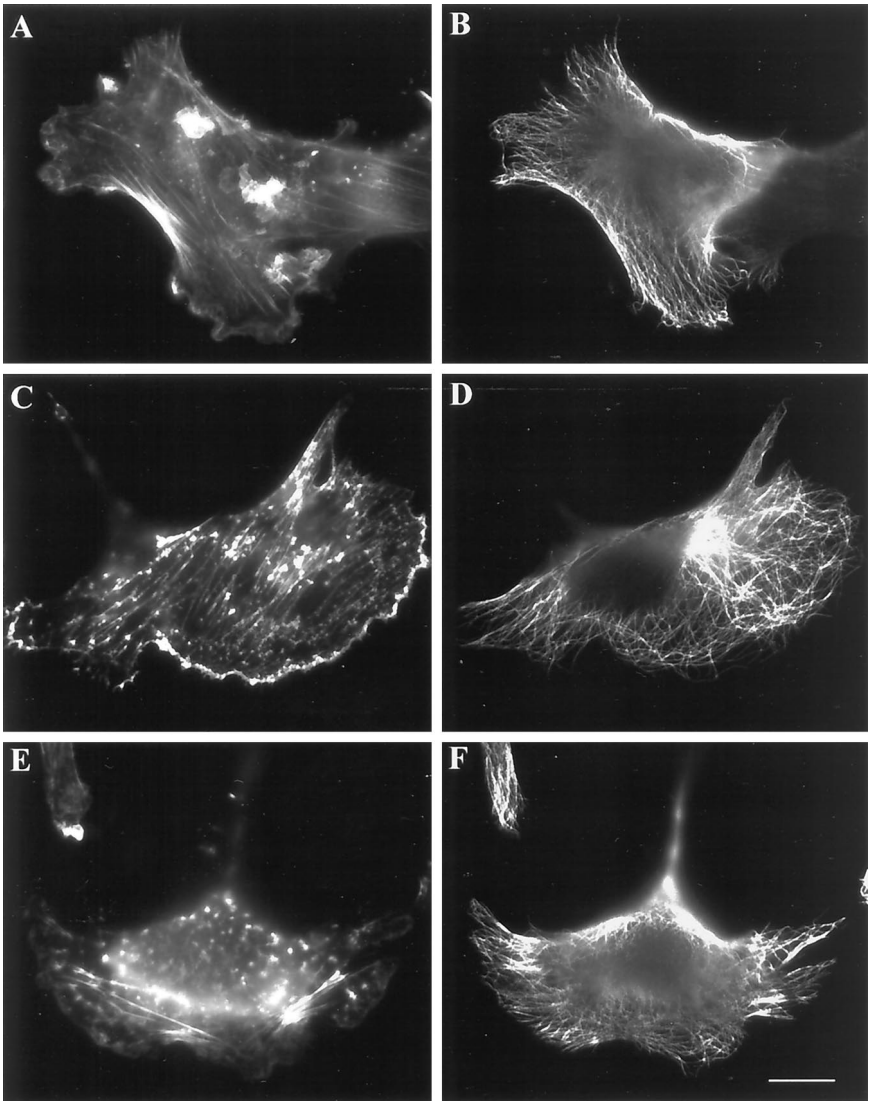

Figure 4. Drugs that disorganize actin filaments do not affect microtubules organization. BWTG3 cells were labeled with fluorescent phalloidin (A, C, E) and antitubulin antibody (B, D, F) without treatment (A, B), after 15 min incubation at 37°C with 1 μM cytochalasin D (C, D), or 10 min incubation at 37° with 0,5 μM latrunculin A (E, F). Bar = 10 μm.

the cell shown Figure 2, and similarly for other cells analyzed under the same conditions. Random motions are generally classified into three categories: diffusion, confined diffusion, and a combination of diffusion and directed motion. Mean square displacement of a particle as a function of time is usually well described by equation (2) when the particle is undergoing diffusion and/or a combination of diffusion and directed motion (with $v = 0$ for diffusion). On the other hand, mean square displacement as a function of time, which does not fit equation (2) might indicate a confined diffusion of the particle (Abney *et al.*, 1999), (see Figures 2E and 2F for examples of lysosomes undergoing diffusion [particle number 8], a combination of diffusion and directed motion [particle number 7], and confined diffusion [particle number 6]). Twenty-one percent of the total population of lysosomes from the cells shown Figure 2, and 22% of 290 lysosomes analyzed from three different cells have a mean square displacement with a curvature opposite to the curvature predicted by equation (2) and could not be fitted by it (Table 1). These observations suggest that these lysosomes were confined in a region near their initial tracking point and were probably often immobile in our experimental conditions.

Lysosome pauses could last several seconds (Figure 2C, and video 2C particle 1, Figure 2D and video 2D particle 5) and were often accompanied by shifts in direction (Figure 2D and video 2D, particle 5). Interestingly, some pepstatin A filled compartments at the cell periphery seemed to stop transiently on actin cables (Figure 2D and video 2D particles 4, 5 and 6, see also corresponding tracks on Figure 2E, particles 4, 5 and 6).

In conclusion, our observations indicate that most lysosomes are highly dynamic particles whose rapid bidirectional movements are microtubule-dependent. However, they sometimes transiently stop moving, and some of them can't even diffuse: they are confined. This suggests that a mechanism might exist to immobilize lysosomes at different steps of their traveling along microtubules.

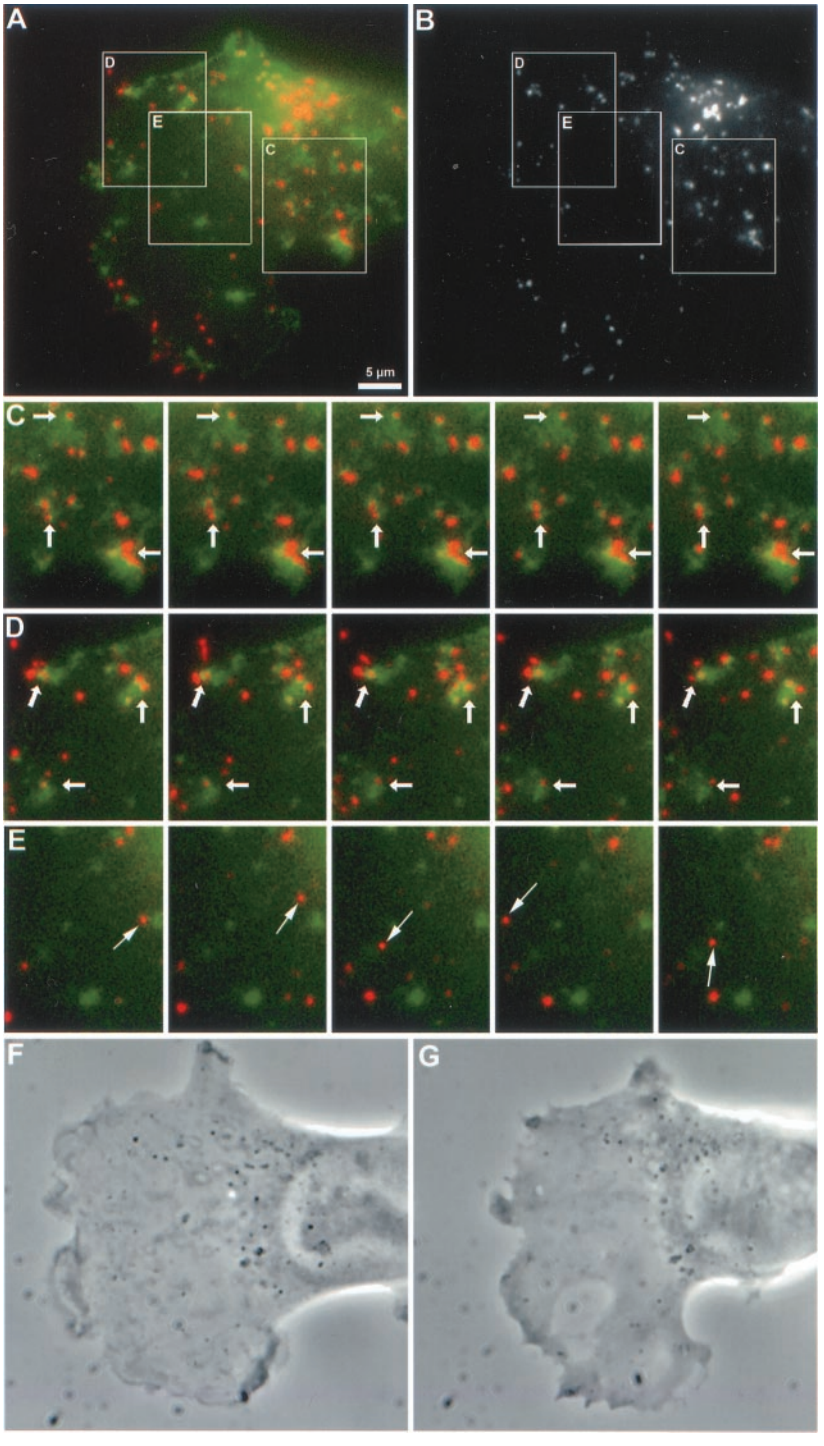

Figure 5. Cytochalasin D treatment immobilizes BODIPY-TR pepstatin A-filled compartments in actin patches in a cell producing GFP-actin. (A) and (B) first frames of time-lapse sequences presented in (C), (D), and (E) after 10 min of cytochalasin D treatment. (A) shows the merge GFP-actin and BODIPY-TR pepstatin A images and (B) BODIPY-TR the pepstatin A image. (C) BODIPY-TR pepstatin A (red) and GFP-actin (green) time-lapse sequence in the perinuclear region of the cell shown in A and B. (D) BODIPY-TR pepstatin A (red) and GFP-actin (green) time-lapse sequence in peripheral region of the cell shown in A and B. Arrows point out fluorescent compartments (red) trapped in actin patches (green). (E) example of fluorescent compartments not trapped in actin patches. Arrows point out one of them that exhibits large random movements. To emphasize the immobility of pepstatin A-filled compartments and actin patches, only one image, approximately every 24 s, was presented from the time-lapse sequences. (F) phase contrast image of the cell before cytochalasin D treatment. (G) phase contrast image of the cell after cytochalasin D treatment, just at the beginning of the time-lapse sequence shown in (C), (D), and (E). Bar = 5 μm.

Actin Filaments Contribute to the Movement of Lysosomes

Since some of the pepstatin A filled compartments at the cell periphery seemed to stop transiently on actin cables we were wondering whether actin filaments could contribute to the movement of lysosomes. We studied by time-lapse video microscopy the behavior of BODIPY-TR pepstatin A filled compartments in presence of 2 drugs, cytochalasin D and latrunculin A that perturb actin cytoskeleton.

Cytochalasin D binds to the barbed end of actin filaments and therefore, by competing with endogenous actin capping proteins, affects the organization of actin cytoskeleton (Cooper, 1987). The addition of 1 μM cytochalasin D to BWTG3 cells or BWTG3 cells expressing GFP-actin during 15 min led to a rapid reorganization of F-actin into amorphous patches dispersed throughout the cytoplasm (Figures 4C, and 5A). However this treatment did not affect neither the gross morphology of the cell (Figures 5F vs. 5G) nor the intracytoplasmic organization of microtubules (Figure 4D). After 10 min of drug treatment, more than 65% of the pepstatin A filled compartments were not moving further than 2.5 μm from their initial tracking point (Table 1, Figure 6A) and were localized with actin patches (Figure 5A). Both actin patches and the pepstatin A filled compartments were animated by movements that seemed to be correlated suggesting that pepstatin A labeled structures were trapped in actin patches (Figures 5C, 5D, and video 5). Indeed, mean square displacement analysis revealed that 50% of the lysosomes were confined (Table 1). As a consequence, the percentage of fluorescent compartments with speeds superior to 0.3 μm/s decreased after drug treatment (Table 1, and Figure 6B). Interestingly, the fluorescent compartments not trapped in actin patches were undergoing a quick succession of rapid multi-directional movements (Figure 5E and video 5), for which the average of the speeds superior to 0.3 μm/s was similar to that calculated in control cells (0.44 $\pm$ 0.02 μm/s, for 49 lysosomes from 3 different cells compared with 0.45 $\pm$ 0.01 for 150 lysosomes of non treated cells). In agreement with the experiment analyzing the dynamic of lysosomes in control cells, this experiment indicates that lysosomes can transiently be immobile when they are in proximity to actin filaments.

Latrunculin A is a drug that binds actin monomers, and as a consequence moves the F-actin/G-actin equilibrium in cells toward G-actin (Lyubimova *et al.*, 1997). After 10 min of treatment actin filaments of BWTG3 cells were partially depolymerized (Figure 4E vs. Figure 4A) but microtubules were still preserved (Figure 4F vs. Figure 4B). Since this treatment increased the intracellular pool of nonpolymerized actin it was more difficult to detect GFP-actin filaments in living BWTG3 cells expressing GFP-actin. GFP-actin staining was diffuse throughout the cytoplasm (Figure 7A). Most of the pepstatin A filled compartments were highly dynamic under these conditions, undergoing a quick succession of rapid movements in random directions (Figures 7C, 7D, Video 7), which made them difficult to track, or even impossible for the most dynamic ones (more than 84% lysosomes were lost during the time-lapse sequence, vs. 57% in the case of control cells). They were also more often elongated than in nontreated cells (7D, arrow, and Figures 7B vs. 2B). The analysis of the trajectories of tractable compartments did not allow us to obtain data that could reasonably be compared with those calculated for control cells.

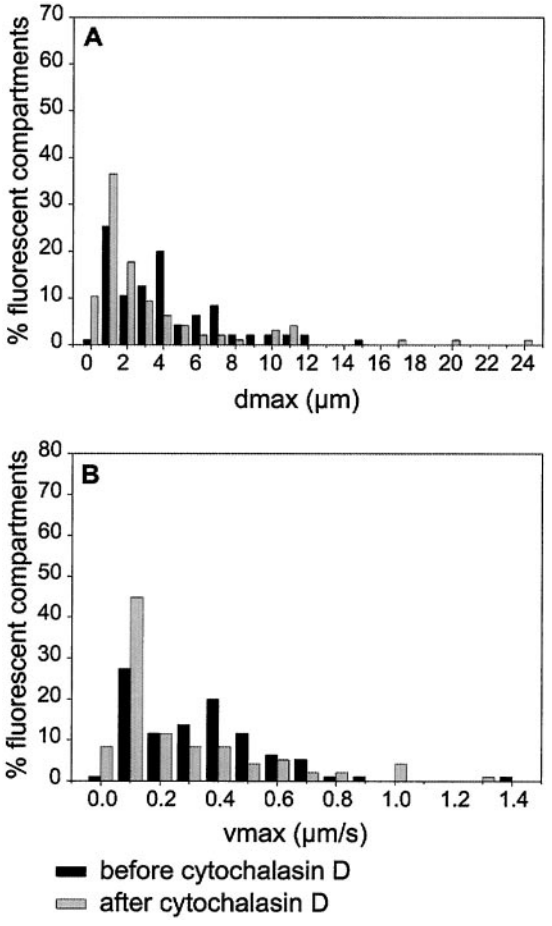

Figure 6. Analysis of the distribution of maximal displacements and maximum speeds recorded for BODIPY-TR pepstatin A filled compartments of a cell producing GFP-actin, before and after addition of cytochalasin D. (A) and (B) show, respectively, the distribution of maximal displacements *dmax* within 3 min and the distribution of maximum speeds *vmax*, before (black bars) and after (gray bars) cytochalasin D treatment. Ninety-five and 96 fluorescent particles were tracked before and after drug treatment, respectively. The number of fluorescent particles with a given *dmax* or *vmax* was calculated as a percentage of the total number of fluorescent particles analyzed.

Latrunculin A, decreases the probability for lysosomes to bind actin filaments by inducing actin depolymerization. In these conditions, lysosomes still move rapidly, but do not favor any particular direction.

Altogether these experiments in agreement with our hypothesis indicate that drugs that perturb the integrity of actin network affect the movement of lysosomes. F-actin network might contribute to the persistence of lysosome directionality by retaining transiently these compartments at special steps of their movement along microtubules.

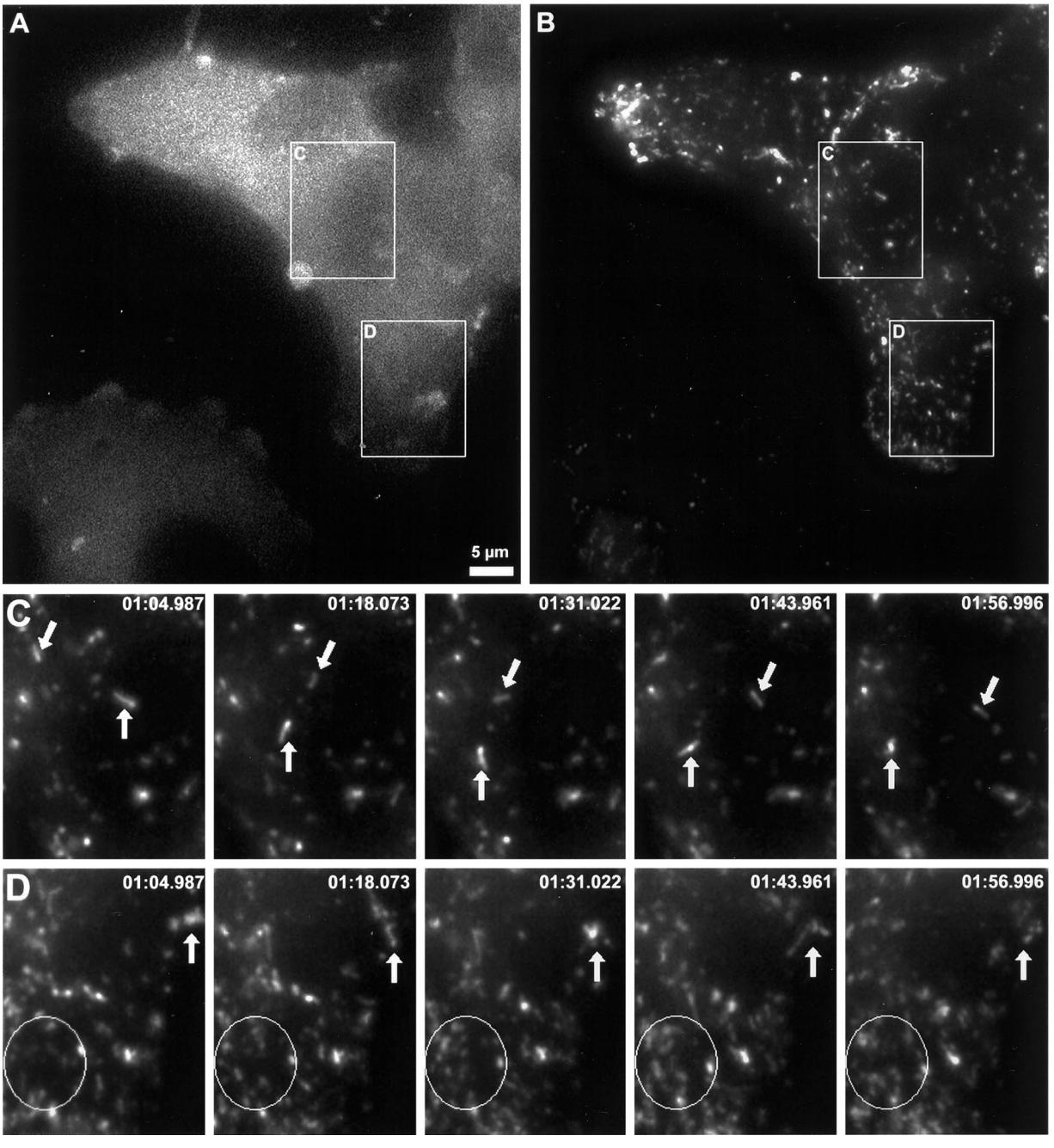

Figure 7. Latrunculin A treatment induces rapid BODIPY-TR pepstatin A filled compartment movements with a loss of directionality in a cell producing GFP-actin. (A) and (B), respectively, show GFP-actin and BODIPY-TR pepstatin A images corresponding to the first frame of the BODIPY-TR pepstatin A time-lapse sequences presented in (C) and (D), 5 min after latrunculin A addition. (C): Time-lapse sequence (one image every 12 s) showing two dynamic elongated BODIPY-TR pepstatin A-filled compartments with no real directionality in the perinuclear region (arrows). (D):Time-lapse sequence (one image every 12 s) showing a peripheral region where BODIPY-TR pepstatin A-filled compartments are so dynamic that they can't be followed individually (circle), and a BODIPY-TR pepstatin A-filled compartment changing shape very quickly (arrow). Bar = 5 μm.

The Overexpression of GFP-MMIαΔn295 Protein Affects the Association of Endogenous MMIα to Membrane Fractions

We have previously shown that MMIα, one member of the class I myosins family, controls the delivery of internalized molecules from late endosomes to lysosomes (Raposo *et al.*, 1999). Thus we analyzed whether this molecular motor was involved in the movement of lysosomes. Since we have previously observed that transient transfection of a cDNA encoding a GFP-truncated MMIα, GFP-MMIαΔn295, affects the cellular distribution of endocytic compartments (Raposo *et al.*, 1999), we established a permanent cell line producing this GFP-MMIα mutant to analyze its effect on lysosome dynamics.

We first studied the distribution of overexpressed GFP-MMIαΔn295 after cell fractionation. Similarly to the endogenous MMIα, a fraction of GFP-MMIαΔn295 was detected in the pellet after centrifugation of the postnuclear supernatant, suggesting that GFP-MMIαΔn295 was associated with cellular membranes (Figure 8A, column PΔ, lane 1 and 2). Moreover, like the endogenous protein, GFP-MMIαΔn295 was associated with the different membrane fractions (Figure 8B, GFP-MMIαΔn295 cells, columns P1, P2, P3, lane 1), including the lysosomal fraction (Figure 8B, GFP-MMIαΔn295 cells, column P1, lane 1 vs. lane 3), isolated on Percoll gradient from the PNS of GFP-MMIαΔn295 expressing cells. In contrast, most of the GFP was detected in the soluble cytosolic fraction of the PNS derived from cells producing the GFP alone (Figure 8A, column Sg, lane 1). Interestingly, endogenous MMIα was detected in the cytosolic fraction of the PNS prepared with GFP-MMIαΔn295 expressing cells (Figure 8A, column SΔ, lane 2), while it was barely observed in the cytosolic fraction of the PNS derived from cells producing GFP (Figure 8A, column Sg, lane 2), or wild-type cells (Raposo *et al.*, 1999). All together, these data suggest that GFP-MMIαΔn295, lacking a domain that encompasses the ATP binding site, is associated with lysosomes similarly to the wild-type protein. Moreover, it can compete with endogenous MMIα and dissociate it from cellular membranes, including these organelles.

Overexpression of GFP-MMIαΔn295 Affects Lysosome Movement

To determine the contribution of MMIα in the motion of lysosomes, we studied the movements of pepstatin A filled compartments in BWTG3 cells stably expressing GFP-MMIαΔn295. The intracellular distribution of GFP-MMIαΔn295 observed by immunofluorescence microscopy gave rise to a diffuse pattern throughout the cytoplasm of fixed or living cells (Raposo *et al.*, 1999, and Figure 9A), which may correspond to the protein detected in the supernatant after centrifugation of the PNS (Figure 8A, column SΔ, lane 1). Like in wild-type cells or cells producing GFP, GFP-MMIα or GFP-actin, internalized BODIPY-TR pepstatin A gave rise to a punctate staining in the cytoplasm that codistributed with Lamp1 in cells producing GFP-MMIαΔn295 (our unpublished results). As previously observed after transient transfection, lysosomes were mainly localized in the juxta-nuclear region in contrast to their dispersed distribution in control cells (Figures 9B and 11C vs. Figures 1B, 2B and 11A). Interestingly, fluorescent lysosomes were larger than lysosomes in wild-type cells (Figures 9A, particles in circle 2, vs. 2C, particles 1, 2, and 3). Their movements seem to be correlated that might suggests that they are connected with neighboring fluorescent lysosomes (Figure 9C, and video 9).

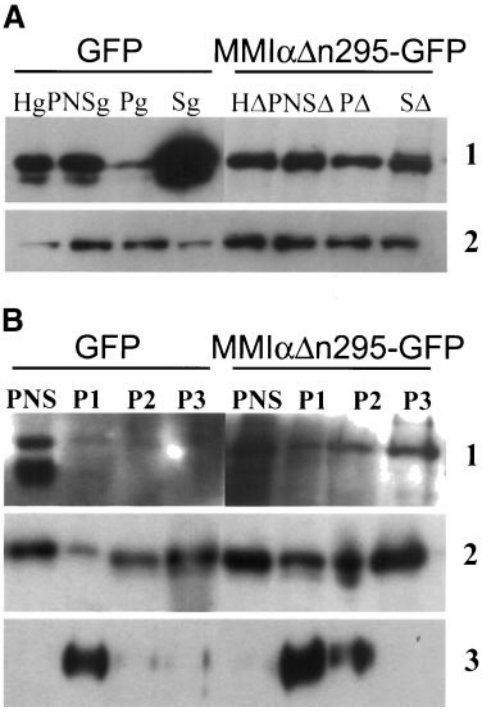

Figure 8. Detection of MMIα or GFP-MM IαΔn295 in the subcellular fraction of BWTG3 cells producing GFP or GFP-MM IαΔn295. (A) Postnuclear supernatants of both cell lines were centrifuged 30 min at 300,000 × *g*, and pellets and supernatants were collected. Ten micrograms homogenate (Hg, HΔ), PNS (PNSg, PNSΔ), protein from the pellet equivalent to 10 μg PNS (Pg, PΔ), and protein from the supernatant equivalent to 100 micrograms of PNS (Sg, SΔ) were separated by 7.5% SDS-PAGE and transferred onto nitrocellulose membranes. The membranes were probed with anti-GFP (lane 1) and anti-MMIα antibodies (lane 2). (B) Fractions collected after separation by Percoll density gradient of the PNS from both cell lines were combined together into three pools, separating lysosomes from endosomes and plasma membranes, as already described for wild-type cells (Raposo *et al.*, 1999). The same amount of protein of each pool (P1, P2, P3) was loaded on 7.5% SDS-PAGE, together with the same amount of protein of the related PNS (PNS) and were analyzed by immunoblotting with anti-GFP (lane 1), anti-MMIα (lane 2), and anti-Lamp1 antibodies (lane 3). The fraction shown in P1 is enriched for the lysosomal marker and exhibits also the endogenous MMIα and GFP-MM IαΔn295.

Most of the pepstatin A filled compartments in GFP-MMIαΔn295 expressing cells were undergoing either short random motions or a quick succession of short linear movements in all directions (Figures 9C, 9D, and video 9). This phenotype has been observed in 3 different cellular clones of BWTG3 cells producing GFP-MMIαΔn295. The proportion of lysosomes traveling <2.5 μm from their initial tracking point was similar to the proportion observed in cells producing GFP-actin (Table 1). The percentage of confined lysosomes, as analyzed by mean square displacement study,

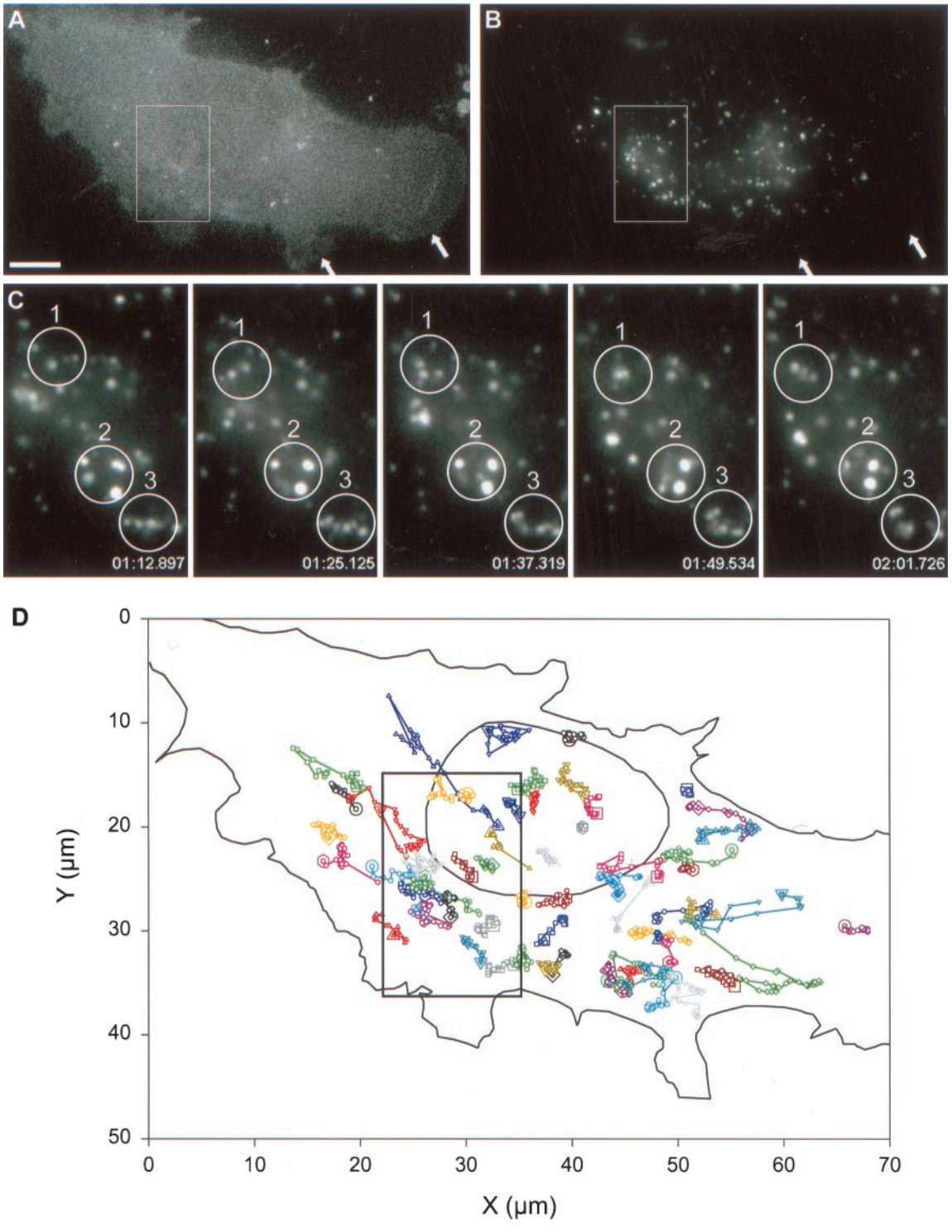

Figure 9. Analysis of the movement of BODIPY-TR pepstatin A filled compartments in cells producing GFP-MM IαΔn295 by time-lapse video microscopy. Thirty-one couples of GFP/Texas Red images were captured at a rate of one couple every 6 s for a cell producing GFP-MM IαΔn295 after BODIPY-TR pepstatin A internalization. (A) First GFP-MM IαΔn295 of the time-lapse sequence. (B): First BODIPY-TR pepstatin A frame of the time-lapse sequence. The white arrows in B indicate the cell periphery, empty of lysosomes. (C) Pepstatin A time-lapse sequence in the rectangle area shown in panels A and B at a rate of one image every 12s (the exact time is given on the pictures), showing that vesicle movements are limited or perturbed by neighboring vesicles. The circles 1, 2, 3 show regions where lysosomes seem to be influenced by each other. (D) Examples of trajectories of pepstatin A-filled compartments in the cell shown in A and B, tracked under the same conditions as for Figure 2. Bar = 10 μm.

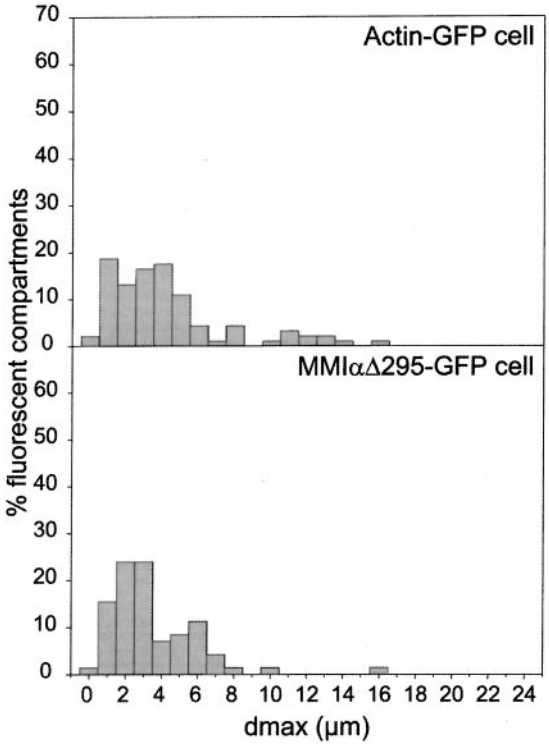

Figure 10. Analysis of the distribution of maximal displacements recorded for BODIPY-TR pepstatin A-filled compartments of cells producing GFP-actin and GFP-MM IαΔn295. The cells analyzed here are the two cells described in Figure 2, and 9. Ninety-one and 71 fluorescent particles, respectively, were tracked in the cells producing GFP-actin and GFP-MM IαΔn295 respectively. The number of fluorescent particles with a given *dmax* within 3 min is calculated as a percentage of the total number of fluorescent particles analyzed. Twice more BODIPY-TR pepstatin A filled compartments have a *dmax* higher than 6.5 μm in actin-GFP cells than in GFP-MM IαΔn295.

was comparable to the percentage of confined lysosomes in cells producing GFP-actin. The mean of microtubule-dependent speeds was also similar to the one calculated for cells producing GFP-actin (0.44 ± 0.01 μm/s, mean from 202 lysosomes taken in 5 different cells). However, long-range directional movement of fluorescent compartments seemed to be less frequent and maximum displacements were shorter compared with the corresponding maximum displacements observed in cells producing GFP-actin. 6% of these lysosomes went further than 8.5 μm, against 12% in GFP-actin expressing cells (these values were calculated for the lysosomes of 3 different cells in each case). Figure 10 shows an example of the distribution of the maximum displacements of one GFP-actin expressing cell vs. one GFP-MMIαΔn295 expressing cell. Maximum displacements within 3 min decreased in the case of the GFP-MMIαΔn295 expressing cell compared with the GFP-actin expressing cell. These changes detected in lysosome behavior gave rise to a global increase in the length of the trajectory used to travel between 2 points. This phenomenon can also be described by the persistence of lysosomes (see Equation 1): lysosome persistence is 1 when the vesicle goes straight from the initial point to the final point. An increase in the length of the trajectory between the same 2 points corresponds to a larger persistence. Indeed, persistence of lysosomes going further than 2.5 μm from their initial tracking point was 4.62 ± 0.45 in cells producing GFP-actin (192 lysosomes going further than 2.5 μm from 3 different cells were analyzed), vs. 6.22 ± 0.42 in GFP-MMIαΔn295 expressing cells (248 lysosomes going further than 2.5 μm from 5 different cells were analyzed). Those 2 values of persistence are significantly different (student *t* test successful, with p = 0.01, and 438 degrees of freedom).

To determine if these disorganized movements were still microtubules-dependent, we treated GFP-MMIαΔn295 expressing cells with nocodazole. After 10 min of treatment, the succession of random directional movements was inhibited, and replaced by short random movements comparable to those observed after nocodazole treatment in GFP actin expressing cells. The average speed and maximum speed were 0.030 ± 0.001 μm/s and 0.090 ± 0.006 μm/s, respectively for GFP-MMIαΔn295 expressing cells treated with nocodazole vs. 0.023 ± 0.001 μm/s and 0.081 ± 0.005 μm/s for GFP-actin expressing cells treated with nocodazole (Figure 11, and Table 1).

GFP-MMIαΔn295 is deleted in the amino-terminus for the actin-binding site but still exhibits the putative sequence for the actin-binding site. Thus we were wondering whether the effect of GFP-MMIαΔn295 was direct or indirect via the desorganization of the actin cytoskeleton. We compared the distribution of actin and microtubules in cells producing GFP-MMIαΔn295 to their distribution in mock cells. The distribution of actin filaments decorated in these cells by fluorescent phalloidin was similar to their distribution in cells producing GFP (Figure 12E vs. F). Furthermore the distribution of microtubules was also similar in both cell types (Figure 12G vs. H).

All together these experiments indicate that GFP-MMIαΔn295 mutant affects lysosome long-range movements although lysosomes disorganized movements are still processed along microtubules.

DISCUSSION

We investigated in this study the contribution of actin to the movement of one type of endocytic compartment, lysosomes. We observed that lysosomes are highly dynamic tubulo-vesicular structures that move from the cell periphery to the juxta-nuclear region and vice versa. These movements are in keeping with the fact that lysosomes might interact both with the plasma membrane and late endosomes at the cell periphery and in the juxta-nuclear region respectively (Andrews, 2000).

Lysosomes exhibit a combination of rapid long bidirectional movements, short random motions and pauses. Rapid long bidirectional movements with a speed higher than 0.3 μm/s and a distance higher than 2.5 μm are inhibited by nocodazole and thus are microtubule-dependent. The microtubule-dependent average speed of lysosomes calculated here (0.45 ± 0.01 μm/s) is slower than that calculated for the movement of endosomes in hippocampal neurons (0.85 ± 0.1 μm/s, Prekeris *et al.*, 1999). The maximum speed of long-range directional lysosomes (0.66 ± 0.06 μm/s) is also slower than that observed for acidic compartments in NRK

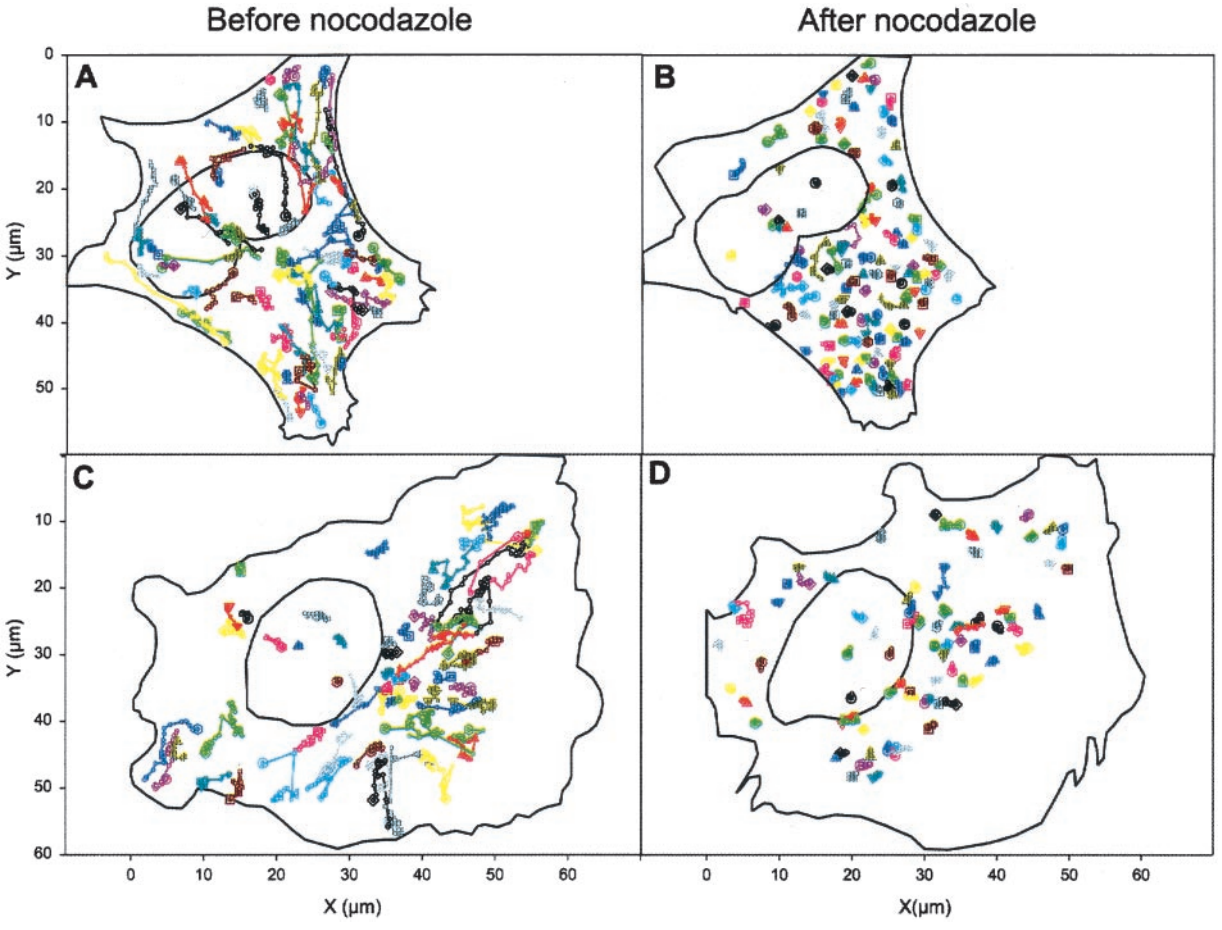

Figure 11. Effect of nocodazole on movements of a BODIPY-TR pepstatin A compartments in GFP-actin and GFP-MM IαΔn295 expressing cells. A and B show examples of trajectories tracked on time-lapse sequences showing the dynamic of BODIPY-TR pepstatin A compartments in cells producing GFP-actin in the absence (A) or after the addition (B) of nocodazole. C and D show examples of trajectories tracked on the time-lapse sequences showing the dynamic of BODIPY-TR pepstatin A compartments in cells producing GFP-MM IαΔn295 in the absence (C) or after the addition (D) of nocodazole. Note that trajectories are distributed throughout the cytoplasm in the control cell while they are concentrated next to the nucleus in the cell producing GFP-MM IαΔn295.

cells (2.5 μm/s) (Matteoni and Kreis, 1987). The reason for these differences is not clear, but may be due to the different methods of calculus used, the difference between the organelles (lysosomes vs. endosomes or acidic compartments), or the cellular origin of the organelle studied. Interestingly, the microtubule-dependent average speed of lysosomes that we have calculated is consistent with the mean velocity of endosomes derived from rat hepatocytes moving along microtubules in vitro (0. 55 $\pm$ 0.23 μm/s, Murray *et al.*, 2000).

The short random motions remaining after nocodazole treatment were much slower than the movement of rocketing lysosomes at the tip of dynamic actin comet tails previously observed in *xenopus* eggs after fertilization or in stimulated mast cells (0.026 μm/s vs. 0.17 and 0.24 μm/s, respectively, Taunton *et al.*, 2000; Merrifield *et al.*, 1999). Furthermore we did not observe in BWTG3 cells, the actin comet tail previously described in ligand activated cells. Therefore actin doesn't seem to be recruited to the membrane of lysosomes to push these organelles through the cytoplasm under our experimental conditions. However since some of the immobile lysosomes were in the vicinity of actin filaments we were wondering whether actin cytoskeleton could contribute to the movements of lysosomes. Indeed we observed that lysosomes are rarely released from the newly formed actin structures after cytochalasin D treatment. Consequently, lysosome movement is considerably reduced under these conditions. Furthermore depolymerization of actin filaments by latrunculin A increases the mobility of tubular lysosomes to such an extend that most of the lysosomes observed at the beginning of the experiment are lost a few seconds later. All together our observations indicate that the F-actin network is involved in the movement of lysosomes. The F-actin network might transiently retain lysosomes during their movement along microtubules. In the absence of F-actin, lysosomes might still move on microtubules but might often be released from them, as observed in vitro by Murray *et al.* (2000), leading to rapid movements in random directions.

Our previous observations suggested that MM Iα contributes to the endocytic process by controlling the delivery of

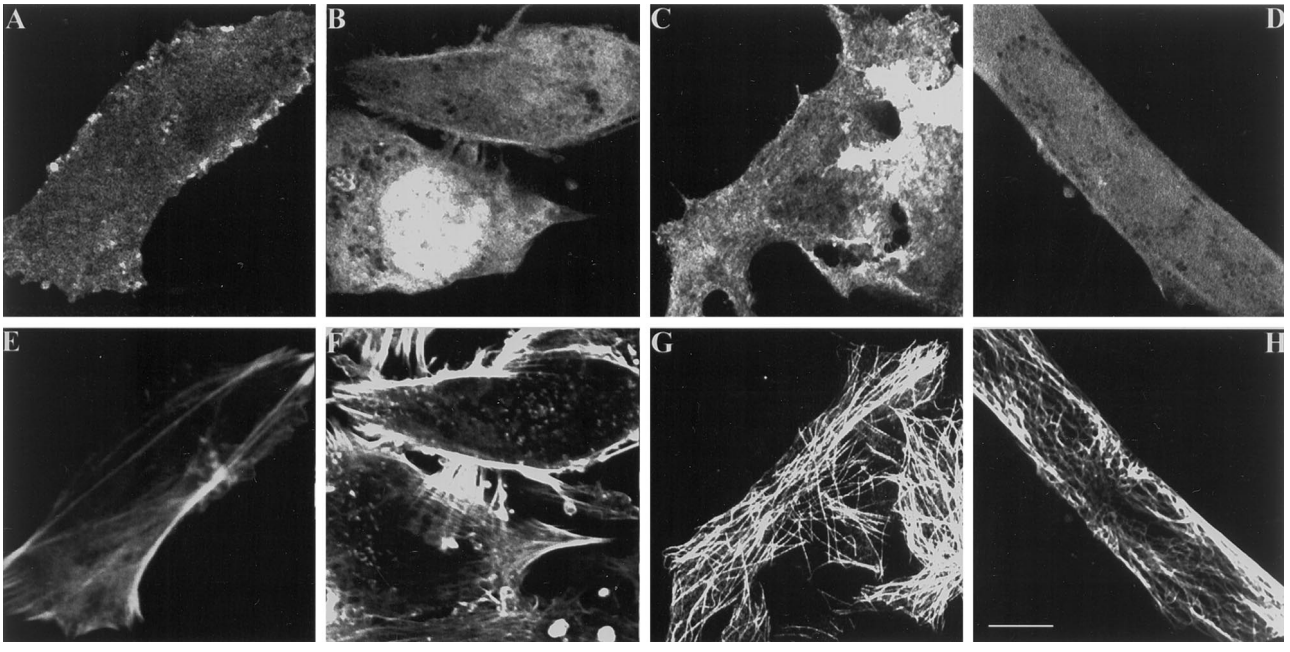

Figure 12. The production of GFP-MM IαΔn295 doesn't affect actin network and microtubule cellular distribution. Cells producing GFP-MM IαΔn295 (A, C, E, and G) or mock cells (B, D, F, and H) were labeled with fluorescent phalloidin (E, F) or anti tubulin antibody (G, H). A, B, C, and D show the cellular distribution of GFP-MM IαΔn295 and GFP, respectively. Bars = 10 μm.

internalized molecules from endosomes to lysosomes (Raposo *et al.*, 1999). Thus we analyzed whether MM Iα could be involved in lysosome movement. We showed that the production of truncated GFP-MM IαΔn295 that lacks the ATP binding site, and is thereby non functional, modifies the dynamic and the distribution of lysosomes. Lysosomes undergo a quick succession of short movements with random directionality that are sensitive to nocodazole in cells producing GFP-MM IαΔn295. Although GFP-MM IαΔn295 still exhibits the actin-binding site it doesn't affect the intracellular distribution of the actin network. The modifications induced by the overproduction of GFP-MM IαΔn295 might therefore be due to a direct effect of the protein on lysosomes rather than an effect on the organization of the actin cytoskeleton. The release of MMIα in the cytosolic fraction of cells producing GFP-MM IαΔn295 suggests that GFP-MMIαΔn295 might have a dominant negative effect on the function of the endogenous MMIα by competing with this protein for its receptor on lysosomes. Altogether these observations might indicate that MMIα contributes to the long-range movements of lysosomes along microtubules. Recent evidence suggests that myosin I from yeast and amoeba might contribute to actin polymerization and actin network organization (Evangelista *et al.*, 2000; Geli *et al.*, 2000; Lee *et al.*, 2000, Jung *et al.* 2001). However, it is unlikely that the contribution of MMIα to the long-range movements of lysosomes is based on such type of molecular mechanism since it doesn't encompass amino acid sequences necessary for this mechanism (a second actin binding site, an SH3 motif or a COOH acidic region similar to the A domain of WASp that binds the Arp 2/3 complex). MMIα, together with the F-actin network, might rather act as part of the regulatory machinery that transiently retains lysosomes during their traveling along microtubules. This hypothesis is in agreement with the kinetic analysis of MMIα indicating that this molecular motor can maintain a tension between cargo and actin filaments rather than move cargoes on actin filaments (Coluccio and Geeves, 1999).

In agreement with previous studies, we observed tubulovesicular lysosomes in nontreated cells (Hopkins *et al.*, 1994; Futter *et al.*, 1998). The change in shape of lysosomes to long tubular structures after latrunculin A treatment, to aggregated structures after cytochalasin D treatment or to connected structures upon production of GFP-MM IαΔn295 is compatible with the involvement of both microtubules and the actin network in maintaining the shape of these organelles. Indeed it has been recently observed that endosomes elongate, and are capable of fission when they bind to microtubules (Bananis *et al.*, 2000). In view of our data, it is tempting to postulate that actin filaments together with MMIα participate in the homotypic fusion of lysosomes and/or heterotypic fusion with late endosomes. This hypothesis is in keeping with the aggregated structures observed when lysosomes are immobilized on actin patches after cytochalasin D treatment and with the larger likely connected vesicles observed after production of GFP-MM IαΔn295. It is also supported by previous observations showing that the delivery of internalized molecules to lysosomes requires the integrity of actin filaments and a functional myosin (Van Deurs *et al.*, 1995; Durrbach *et al.*, 1996a and 1996b; Raposo *et al.*, 1999), and by the cellular distribution of MMIα. Indeed MM Iα has been detected both in the perinuclear region, where fusion events between late endosomes and lysosomes occur, and at the cell periphery, where it might play a role in the fusion of lysosomes with the plasma membrane as suggested by Temesvari *et al.* (1996)

for the myosin Ib in *dictyostellium* (Bucci *et al.*, 2000; Raposo *et al.*, 1999).

Organelle transport has been proposed to proceed along microtubules for long-range transport and *via* actin filaments for local delivery. This model implicates class V myosin as the actin based molecular motor, and is supported by studies of pigment transport in different cell types and transport along the secretory pathway in neurons (Wu *et al.*, 1998; Bridgman, 1999). Our experiments suggest that a second type of regulatory machinery involving actin filaments and a member of class I myosins controls the trajectories of organelles on microtubules and, thus might mediate the cooperation between microtubules, actin and related motors.

ACKNOWLEDGMENTS

We thank Dr. J. B. Sibarita (CNRS Institut Curie) for helpful advice concerning time-lapse video microscopy and image analysis, and Drs. J. Plastino and F. Amblard for critical comments on the manuscript. This work was supported by a grant to E. Coudrier from the Association pour la Recherche sur le Cancer (ARC n° 5459). M.-N. Cordonnier was the recipient of a grant from la Ligue contre le Cancer.

REFERENCES

Abney, J.R., Meliza, C.D., Culer, B., Kingma, M., Locher, J., and Scalettar, B. (1999). Real-time imaging of the dynamics of secretory granules in growth cones. Biophys. J. *77*, 2887–2895.

Andrews, N. (2000). Regulated secretion of conventional lysosomes. Trends Cell Biol. *10*, 316–321.

Aniento, F., Emans, N., Griffiths, G., and Gruenberg, J. (1993). Cytoplasmic Dynein-dependent vesicular transport from early to late endosomes. J. Cell Biol. *123*, 1373–1387.

Ballestrem, B., Wehrle-Haller, B., and Imhof, B.A. (1998). Actin dynamics in living mammalian cells. J. Cell Sci. *111*, 1649–1658.

Bananis, E., Murray, J., Stockert, R., Satir, P., and Wolkoff, A. (2000). Microtubule and motor-dependent endocytic vesicles sorting in vitro. J. Cell Biol. *151*, 179–186.

Barois, N., Forquet, F,., and Davoust, J. (1998). Actin microfilaments control the MHC class II antigen presentation pathway in B cells. J. Cell Sci. *111*, 1791–1800.

Bridgman, P. (1999). Myosin Va movements in normal and dilute-lethal axons provide support for a dual filament motor complex. J. Cell Biol. *146*, 1045–1060.

Bucci, C., Thomsen, P., Nicoziani, P., McCarthy, J., and van Deurs, B. (2000). Rab7: A key to lysosome biogenesis. Mol. Biol. Cell *11*, 467–480.

Chen, C., Chen, W., Zhou, M., Arttamangkul, S., and Haugland, R. (2000). Probing the cathepsin D using a BODIPY FL-pepstatin A: application in fluorescence polarization and microscopy. J. Biochem. Biophys. Meth. *42*, 137–151.

Coluccio, L., and Geeves, M. (1999). Transient kinetic analysis of the 130kDa myosin I(Myr-1gene product) from rat liver. J. Biol. Chem. *274*, 21575–21580.

Cooper, J. (1987). Effects of cytochalasin D and phalloidin on actin. J. Cell Biol. *105*, 1473–1478.

Coudrier, E., Durrbach, A., and Louvard, D. (1992). Do unconventional myosins exert functions in dynamics of membrane compartments? Febs Lett. *307*, 87–92.

Durrbach, A., Louvard, D., and Coudrier, E. (1996a). Actin filaments facilitate two steps of endocytosis. J. Cell Sci. *109*, 457–465.

Durrbach, A., Collins, K., Matsudaira, P., Louvard, D., and Coudrier, E. (1996b). Brush border myosin-1 truncated in the motor domain, impairs the distribution and the function of endocytic compartments in a hepatoma cell line. Proc. Natl. Acad. Sci. USA *93*, 7058–7073.

Evangelista, M., Kleb, B.M., Tong, A.H.Y., Webb, B., Leeuw, T., Leberer, E., Whiteway, M., Thomas, D.Y., and Boone, C. (2000). A role for myosin I in actin assembly through interactions with Vrp1p, bee1p, and the Arp2/3 complex. J. Cell Biol. *148*, 353–362.

Futter, C.E., Pearse, A., Hewlett, L.J., and Hopkins, C.R. (1996). Multivesicular endosomes containing internalized EGF-EGF receptor complexes mature and then fuse directly with lysosomes. J. Cell Biol. *132*, 1011–1023.

Futter, C.E., Gibson, A., Allchin, E.H., Maxwell, S., Ruddock, L.J., Odorizzi, G., Domingo, D., Trowbridge, I.S., and Hopkins, C.R. (1998). In polarized MDCK cells, basolateral vesicles arise from clathrin-γ-adaptin-coated domain on endosomal tubules. J. Cell Biol. *141*, 611–623.

Geli, M.I., and Riezman, H. (1996). Role of type I myosins in receptor-mediated endocytosis in yeast. Science *272*, 533–535.

Geli, I., Lombardi, R., Schmelzl, B., and Riezman, H. (2000). An intact SH3 domain is required for myosin I-induced actin polymerization. EMBO J.*19*, 4281–4291.

Green, S.A., Zimmer, K.-P., Griffiths, G., and Mellman, I. (1987). Kinetics of intracellular transport and sorting of lysosomal membrane and plasma membrane proteins. J. Cell Biol. *105*, 1227–1240.

Hollenbeck, P., and Swanson, J. (1990). Radial extension of macrophage tubular lysosomes supported by kinesin. Nature *346*, 864–6.

Hopkins, C.K., Gibson, A., Shipman, M., Strickland, D.K., and Trowbridge, I.S. (1994). In migrating fibroblasts, recycling receptors are concentrated in narrow tubules in the pericentriolar area, and then routed to the plasma membrane of the leading lamella. J. Cell Biol. *125*, 1265–1274.

Jung, G., Wu, X., and Hammer III, J.A. (1996). Dictyostelium mutants lacking multiple classic myosin I isoforms reveal combination of shared and distinct functions. J. Cell Biol. *133*, 305–323.

Jung, G., K. Remmert, Wu, X, Volosky, J.M., and Hammer III, J.A. (2001). The dictyostellium CARMIL protein links capping protein and the Arp2/3 complex to type I myosins through their SH3 domains. J. Cell Biol. *153*, 1479–1497.

Lee, W.-L., Bezanilla, M., and Pollard, T. (2000). Fission yeast myosin -I, Myo1p, stimulates actin assembly by Arp2/3 complex and shares functions with WASP. J. Cell Biol. *151*, 789–799.

Liu, J., Thomas, L., Warren, R.A., Enns, C.A., Cunningham, C.C., and Hartwig, C.H. (1997). Cytoskeletal protein ABP-280 directs the intracellular trafficking of furin and modulates protein processing in the endocytic pathway. J. Cell Biol. *139*, 1719–1733.

Luzio, J.P., Rous, B.A., Bright, N.A., Pryor, P.R., Mullock, B.M., and Piper, R.C. (2000). Lysosome-endosome fusion and lysosome biogenesis. J. Cell Sci. *113*, 1515–1524.

Lyubimova, A., Bershadsky, A., and Ben-Ze'ev, A. (1997). Autoregulation of actin synthesis responds to monomeric actin levels. J. Cell. Biochem. *65*, 459–478.

Matteoni, R., and Kreis, T.E. (1987). Translocation and clustering of endosomes and lysosomes depends on microtubules. J. Cell Biol. *105*, 1253–1265.

Merrifield, C.J., Moss, S.E., Ballestrem, C., Imhof, B.A., Giese, G., Wunderlich, I., and Almers, W. (1999). Endocytic vesicles move at the tips of actin tails in cultured mast cells. Nat. Cell Biol. *1*, 72–74.

Mullock, B.M., Bright, N.A., Fearon, C.W., Gray, S.R., and Luzio, J.P. (1998). Fusion of lysosomes with late endosomes produces a hybrid organelle of intermediate density and is NSF dependent. J. Cell Biol. *140*, 591–601.

Murray, J.W., Bananis, E., and Wolkoff, A.W. (2000). Reconstitution of ATP-dependent movement of endocytic vesicles along microtubules in vitro: an oscillatory bidirectional process. Mol. Biol. Cell *11*, 419–433.

Neuhaus, E.M., and Soldati, T. (2000). A myosin I is involved in membrane recycling from early endosomes. J. Cell Biol. *150*, 1013–1026.

Novak, K.D., Peterson, M.D., Reedy, M.C., and Titus, M.A. (1995). *Dictyostelium* myosin I double mutants exhibit conditional defects in pinocytosis. J. Cell Biol. *131*, 1205–1221.

Ostap, M.E., and Pollard, T.D. (1996). Overlapping functions of myosin-I isoforms. J. Cell Biol. *133*, 221–224.

Prekeris, R., Foletti, D.L., and Scheller, R.H. (1999). Dynamics of tubulovesicular recycling endosomes in hippocampal neurons. J. Neurosci. *19*, 10324–10337.

Raposo, G., Cordonnier, M.-N., Tenza, D., Menichi, B., Durrbach, A., Louvard, D., and Coudrier, E. (1999). Association of myosin I with endosomes and lysosomes in mammalian cells. Mol. Biol. Cell *10*, 1477–1494.

Ruppert, C., Kroschewski, R., and Bähler, M. (1993). Identification, characterization and cloning of myr 1, a mammalian myosin-1. J. Cell Biol. *120*, 1393–1403.

Stoorvogel, W., Strous, G.J., Geuze, H.J., Oorschot, V., and Schwartz, A.L. (1991). Late endosomes derive from early endosomes by maturation. Cell *65*, 417–427.

Szpirer, C., and Szpirer, J. (1975). A mouse hepatoma cell line which secretes several serum proteins including albumin and α-foetoprotein. Differentiation *4*, 85–91.

Taunton, J., Rowning, B.A., Coughlin, M.L., Wu, M., Moon, R.T., Mitchison, T.J., and Larabell, C.A. (2000). Actin-dependent propulsion of endosomes and lysosomes by recruitment of N-Wasp. J. Cell Biol. *148*, 519–530.

Temesvari, L.A., Bush, J.M., Peterson, M.D., Novak, K.D., Titus, M.A., and Cardelli, J.A. (1996). Examination of the endosomal and lysosomal pathway in dictyostelium discoideum myosin I mutants. J. Cell Sci. *109*, 663–673.

Van Deurs, B., Holm, P., Kayser, L., and Sandvig, K. (1995). Delivery to lysosomes in human carcinoma cell line HEp-2 involves an actin filament-facilitated fusion between mature endosomes and preexisting lysosomes. European J. Cell Biol. *66*, 309–323.

White, S., Miller, K., Hopkins, C., and Trowbridge, I.S. (1992). Monoclonal antibodies against defined epitopes of the human transferrin receptor cytoplasmic tail. Biochem. Biophys. Acta *1136*, 28–34.

Wu, X., Bowers, B., Rao, K., Wei, Q., and Hammer III, J.A. (1998). Visualization of melanosomes dynamics within wild-type and dilute melanocytes suggests a paradigm for myosin V function in vivo. J. Cell Biol. *143*, 1899–1918.

Yamashita, R., and May, G. (1998). Constitutive activation of endocytosis by mutation of myoA, the myosin I gene of Aspergillus nidulans. J. Biol. Chem. *273*, 14644–14648.